Molecular dynamics simulations of the solid phase epitaxy of Si : growth mechanism and orientation effects

E. Lampin, Christophe Krzeminski

Molecular dynamics simulations of the solid phase epitaxy of Si: Growth mechanism and orientation effects

Cite as: J. Appl. Phys. **106**, 063519 (2009); https://doi.org/10.1063/1.3211972
Submitted: 03 July 2009 • Accepted: 29 July 2009 • Published Online: 23 September 2009

E. Lampin and C. Krzeminski

Molecular dynamics simulations of the solid phase epitaxy of Si: Growth mechanism and orientation effects

E. Lampin[a] and C. Krzeminski
IEMN, Avenue Poincaré, 59652 Villeneuve d'Ascq Cedex, France

(Received 3 July 2009; accepted 29 July 2009; published online 23 September 2009)

The solid phase epitaxy of an amorphous layer on crystalline silicon is studied by means of molecular dynamics. Three stacks of 5120, 4928, and 5184 atoms respectively oriented along the [100], [110], and [111] directions are annealed with the Tersoff interatomic potential. The regrowth proceeds via the motion of a planar interface for [100], the formation of facets for [110], and the crystallization within (111) bilayers for the third case. In the absence of crystallization defects, the velocities of regrowth are similar for [100] and [110] and two to five times lower for [111]. Moreover, defects were obtained in 8% of the cases along [100], 19% of the cases along [110], and 52% of the cases along [111] with a systematic formation of one or more twins in the last case. The results are confronted with a schematic model of the solid phase epitaxy. © *2009 American Institute of Physics*. [doi:10.1063/1.3211972]

I. INTRODUCTION

The solid phase epitaxy (SPE) of amorphous silicon (*a*-Si) deposited on crystalline silicon (*c*-Si) or formed by high dose bombardment of *c*-Si has been the subject of intensive experiments. In particular, Olson and Roth[1] developed a dedicated technique of interferometry to extract the velocity of regrowth with a good control of the temperature. Their studies were restricted to (100) substrates. The impact of the substrate orientation on the SPE was first studied some time before by Csepregi *et al.*[2] They measured the velocity of SPE at 20 various angles with a technique of backscattering. Their results are widely cited in the literature. Although their contribution is less known, Drosd and Washburn[3] also made some measurements by microscopy on (100), (110), and (111) substrates. The velocities of SPE obtained by the three groups are reported in Fig. 1. The dispersion up to a factor of 10 is probably due to a weak control of the purity and annealing temperature of the sample compared to nowadays technological capabilities. The amorphous layers studied by the authors have micrometric thickness, and their characterization is mostly macroscopic. As pointed out by Johnson *et al.*,[4] the method of the molecular dynamics using interatomic potentials is of particular interest for the modeling of SPE. Preliminary studies on diffusion mechanisms in the crystalline part[5] or defect formation processes during the regrowth of a (100) interface[6] were reported. We propose in this paper to study the details of the SPE at the atomic level in three orientations, (100), (110), and (111), in order to obtain more information on the mechanism of regrowth, on the velocities of SPE, and on the occurrence and nature of the defects generated by crystallization.

The paper is organized as follows: The details of the method used to build *a*-Si on *c*-Si stacks, simulate their annealing, and exploit the simulations are given in Sec. II. The mechanism of regrowth in the three directions is reported in Sec. III, while the SPE velocities and the defects of crystallization are presented in Secs. IV and V. Finally, the results are discussed in Sec. VI. before concluding in Sec. VII.

II. METHOD

First, an atomic stack of *a*-Si on *c*-Si has to be constructed. In a former work,[7] the starting amorphous cluster was obtained by a bond switching method following Wooten *et al.*[8] The motivation was to start from a unique structure to determine the most adapted interatomic potential for the study of SPE. It was found that the Tersoff potential[9] and a modified Stillinger–Weber potential called SW115 (Ref. 10) were the only ones that did not transform amorphous silicon into a liquid. The Tersoff potential was chosen for the better agreement of the regrowth velocity with Olson measurements (see Fig. 2). The weakness of the potential is, however, a shift in the melting temperature to 2500 K that should be accounted for any comparison with experiments. Since the potential is fixed in the present study, we decided to

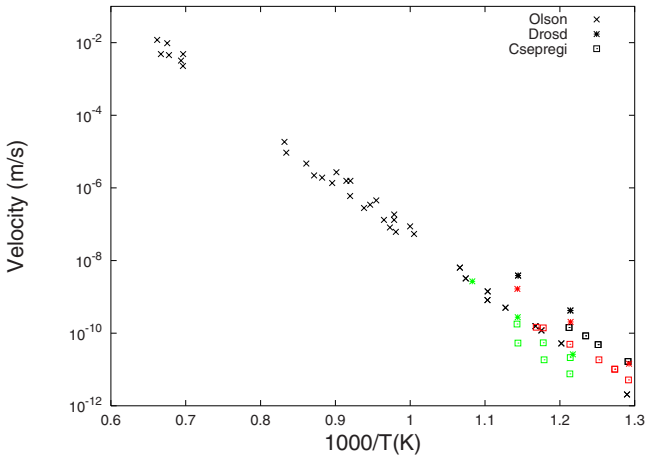

FIG. 1. (Color online) Experimental SPE velocities reported in Refs. 1–3. The symbols in black are for (100), those in red are for (110), and those in green are for (111).

[a]Electronic mail: evelyne.lampin@isen.iemn.univ-lille1.fr.

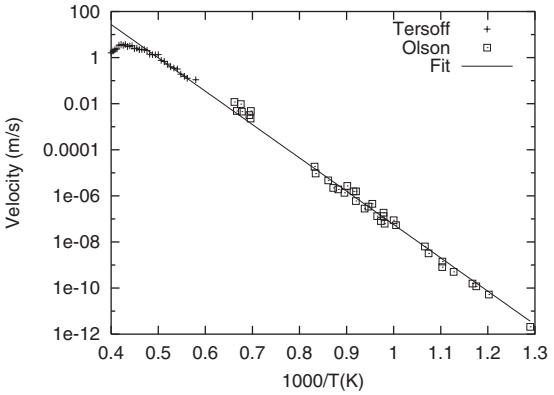

FIG. 2. Regrowth velocity along [100]. Simulation (Tersoff, cross), experiment (Olson, square), and common Arrhenius fit below 2000 K (line).

refine the construction of the *a*-Si/*c*-Si stack, and in particular the quality of the interface, using the Tersoff potential to simulate the melting and quenching of the upper part of a crystalline box. The melting was performed at 3500 K during 10 ps and followed by a ramp-down at 10 K/ps. Figure 3 presents the atomic structure of the three stacks constructed along [100], [110], and [111]. The specific orientations used for the representations in Fig. 3 correspond to convenient views used further for the studies of the interface and defects. The [100] and [110] boxes are cubic and contain, respectively, 5120 and 4928 atoms, and their dimensions are $4.3\times4.3\times5.4$ nm^3. The [111] cell is rhombohedral, and its sides measure 4.6, 4.6, and 6.2 nm. It contains 5184 atoms. The number of atoms was increased in comparison to Ref. 7 ($\approx$2000 atoms). Indeed, the velocity of SPE regrowth has already converged with 2000 atoms, but the study of crystallization defects requires an increase in the size of the simulation cell.

The structure factor and angular distribution of the melted-quenched half of the stacks are shown in Fig. 4. The typical features of *a*-Si are evidenced, i.e., a peak of second neighbors in the structure factor and a Gaussian-like angular distribution with a mean value of 109° and a standard deviation of $\pm20°$.

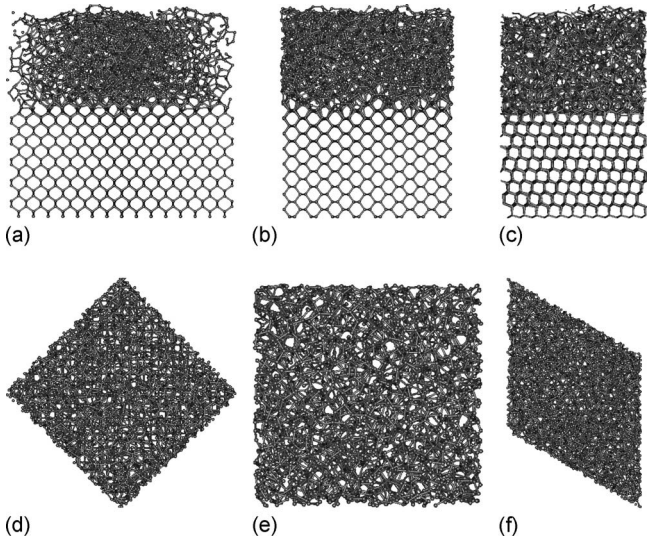

FIG. 3. Amorphous on crystalline stacks of silicon along the [100] (left), [110] (center), and [111] (right) directions.

The molecular dynamics technique is applied to determine the displacement of the atoms upon annealing. After a 4 ps equilibration at the target temperature by scaling the velocities, the temperature is controlled by a Nosé–Hoover[11,12] thermostat. The temperature range is set to [1700–2500 K], the lower limit being fixed by computation limitations and the upper limit by melting. Periodic boundary conditions are applied except in the direction perpendicular to the interface to enable the expansion or contraction of the amorphous material. The atoms of the two planes at the bottom are frozen to their equilibrium position to mimic a semi-infinite structure. During the molecular dynamics calculation, the atomic positions are saved at regular intervals to sample the recrystallization process. The positions are used afterward either for a graphic visualization to identify defects or to extract the regrowth velocity. The regrowth velocity determination is based on the positioning of the *a*-Si/*c*-Si interface. The procedure of Mattoni and Colombo[13] is used to get the interface position. This procedure is based on the calculation of a one-dimensional structure factor:

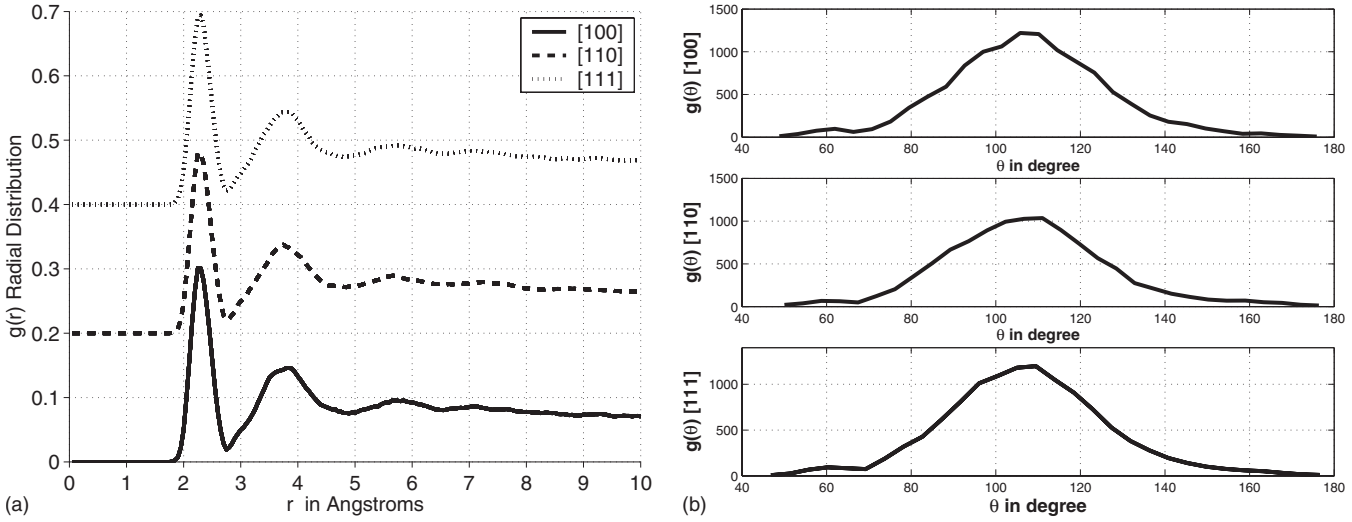

FIG. 4. Radial and angular distributions of the amorphous half of the [100], [110], and [111] boxes.

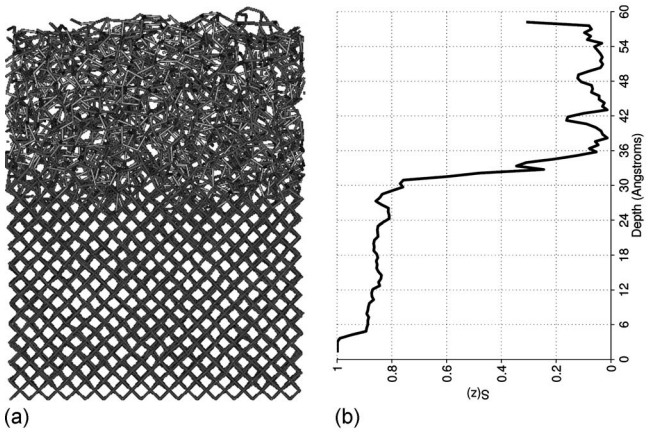

FIG. 5. [100] one-dimensional structure factor.

$$S(z) = \left| \frac{1}{N_z} \sum_{z<z_i<z+dz} \exp(j\vec{k} \cdot \vec{r}_i) \right|, \quad (1)$$

where $\vec{r}_i=(x_i,y_i,z_i)$ denotes the position of atom i, $\vec{k}$ is a vector of the reciprocal lattice parallel to the interface, and N_z is the number of atoms in the layer $[z;z+dz]$ with $dz=2.25$ Å. The values of $\vec{k}$ and dz in the (100), (110), and (111) planes are, respectively,

$$\vec{k}_{100} = \frac{2\pi}{a_0}(\vec{x}+\vec{y}),$$

$$\vec{k}_{110} = \frac{2\pi}{a_0}(\sqrt{2}\vec{x}+\vec{y}),$$

$$\vec{k}_{111} = \frac{2\pi}{a_0}(\sqrt{2}\vec{x}+\sqrt{6}\vec{y}). \quad (2)$$

In addition, $S(z)$ is normalized by a factor of 0.7 for [110]. Figures 5–7 illustrate the correspondence between the order at the atomic level and $S(z)$. The levels of the factor in the crystalline (S above 0.8) and amorphous (S below 0.2) regions are similar in the three cases. The initial transition is rather abrupt (<5 Å), although the interface roughness may further increase upon annealing.

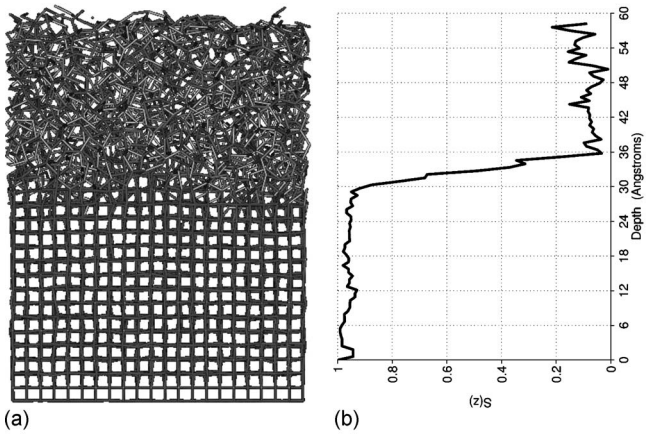

FIG. 6. [110] one-dimensional structure factor.

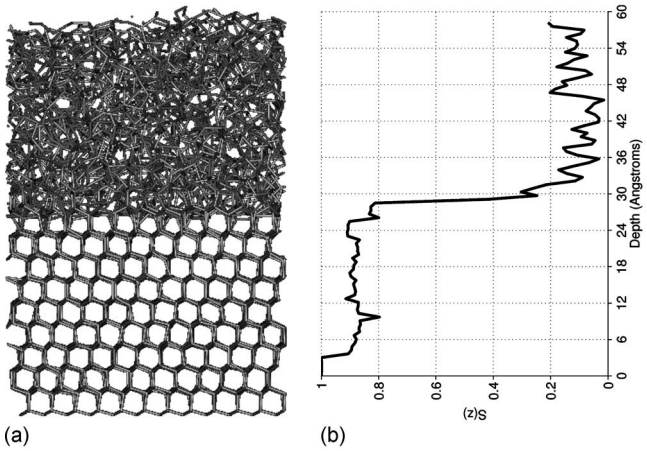

FIG. 7. [111] one-dimensional structure factor.

III. MECHANISM OF REGROWTH

The a-Si/c-Si interface is unstable. Below ≈2500 K, a SPE gradually transforms the amorphous material at the interface into a crystal. At temperatures higher than 2000 K, the amorphous crystalline interface remains abrupt during annealing, and the regrowth progresses toward the surface until the complete transformation into a crystal is achieved. At lower temperatures, the interface roughness is orientation dependent and the regrown layer sometimes contains defects. The differences in terms of the regrowth mechanism are illustrated in Figs. 8–10 for a temperature of 1725 K. On each of these series of pictures, the first image (labeled "Equ.") is obtained after the equilibration step. The other pictures are labeled by the annealing duration.

The a-Si/c-Si interface of the [100] box (Fig. 8) presents little roughness during SPE. The displacement of the

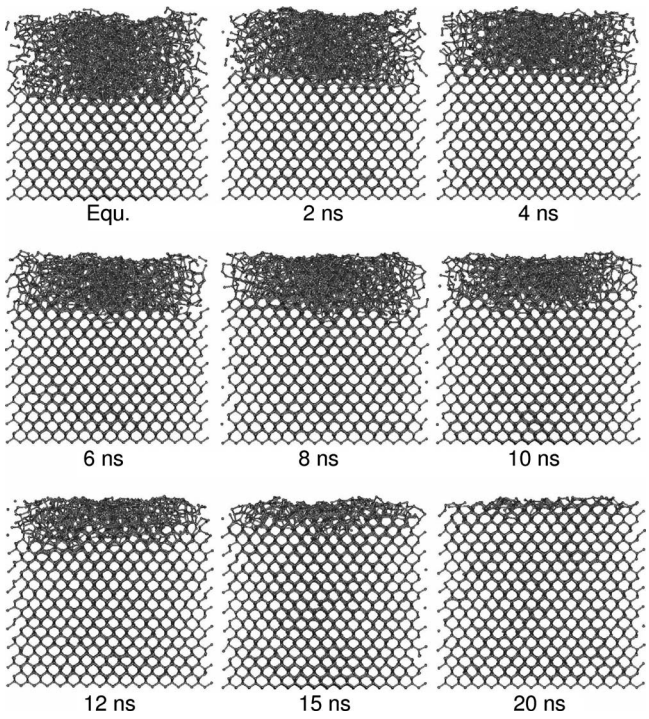

FIG. 8. Evolution of the [100] amorphous on crystalline stack at 1725 K.

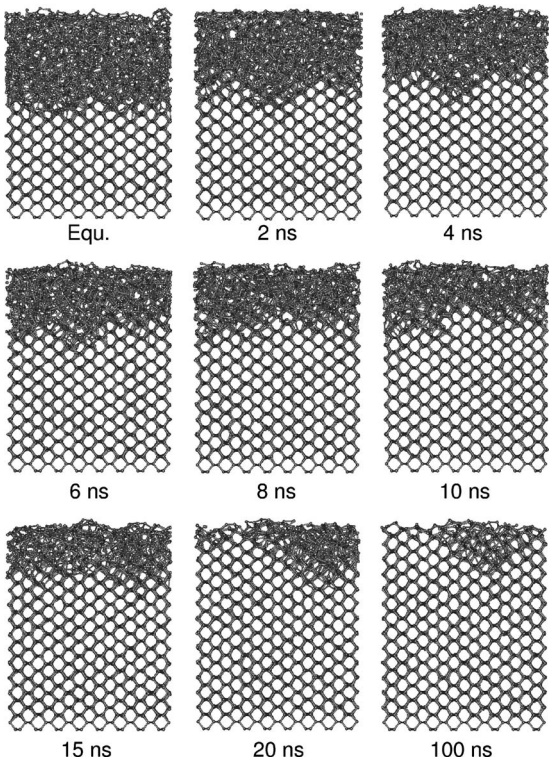

FIG. 9. Evolution of the [110] amorphous on crystalline stack at 1725 K.

a-Si/*c*-Si interface toward the surface shows little deviation to a linear fit (see Fig. 11). In the present example, the final structure is free of defects. Only 8% of the 35 calculations carried out in the range of [1700–2500 K] resulted in the formation of defects.

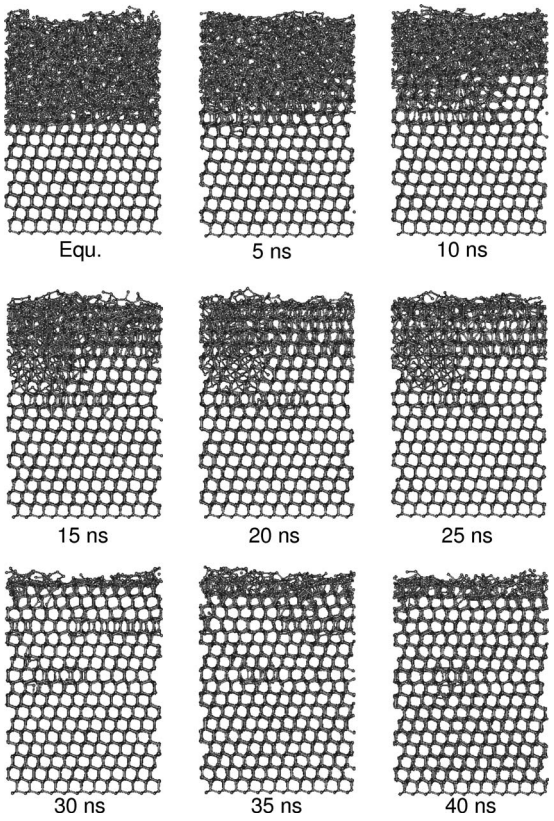

FIG. 10. Evolution of the [111] amorphous on crystalline stack at 1725 K.

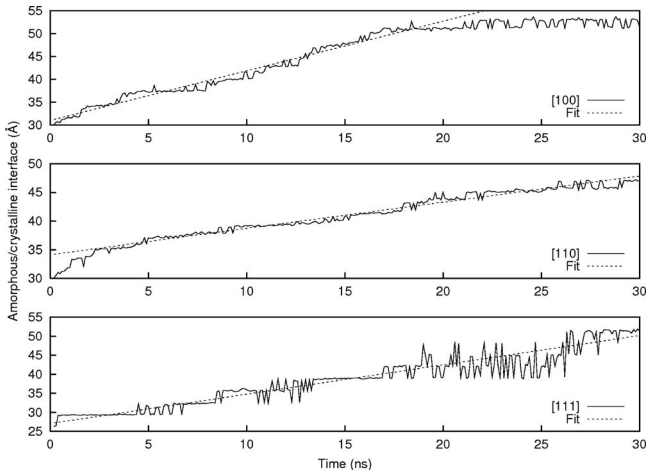

FIG. 11. Position of the amorphous/crystalline interface as a function of time at 1725 K corresponding to Figs. 8–10 and linear regression.

The [110] box has a clear tendency to form [111] facets (Fig. 9). The faceting already starts during the phase of equilibration and becomes particularly pronounced at 2 and 4 ns. Around 6–8 ns, the regrowth mainly progresses by the facets of the prominent amorphous tip, and the roughness of the interface decreases. This succession of sawtooth interface formation/planarization continues until the surface is reached. It may happen, as in this particular case, that a defect forms and remains long after the surface is reached (100 ns). Residual defects generated during the SPE were obtained in 19% of the 42 annealing experiments for the [110] box. The progression of the *a*-Si/*c*-Si interface is almost linear (see Fig. 11) but saturates at a lower value (45 Å) than the [100] box (52 Å) due to the presence of the defect.

The SPE regrowth mechanisms along the [111] direction are even more complex (Fig. 10). The transformation from *a*-Si to *c*-Si occurs by rearrangements of complete or partial bilayers. For example, in the case presented in Fig. 10, a first bilayer is partially formed during the first step of 5 ns. Incomplete bilayers then form on the right part of the structure, while the left part slowly rearranges (10–15 ns) and forms a defect (20–25 ns) that finally cures, letting several crystalline layers (30 ns) to suddenly appear. At this moment, a first twin clearly appears at the tenth bilayer from the bottom, and a defect is visible at the right upper part. The defect is progressively annealed (35 ns) until it disappears (40 ns). A second twin now becomes apparent at the 14th bilayer from the bottom. A buried defect and two disordered bilayers at the top surface remain. The jerky regrowth is also evidenced in Fig. 11. The evolution of the interface is formed of successive plateaus whose height corresponds to the distance (or a multiple of the distance) between (111) bilayers. The formation of one or more twins in (111) planes was observed in nearly all the temperatures simulated (one exception over 42 cases). Other defects are observed in 52% of the simulations.

IV. REGROWTH VELOCITY

The regrowth velocity was extracted for the temperatures where defects are not formed. The velocity is obtained by a linear fit of the *a*-Si/*c*-Si interface position versus time.

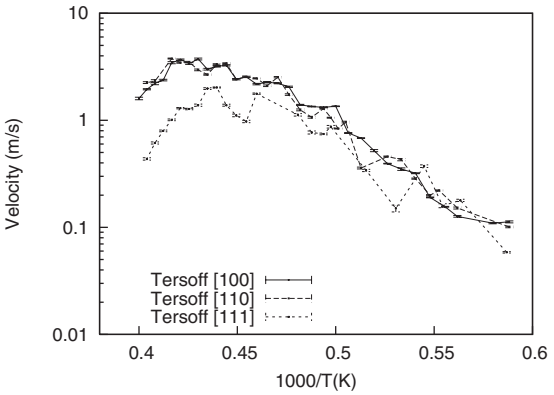

FIG. 12. Regrowth velocity along the [100], [110], and [111] directions. The error bars denote the deviation from a linear dependence of the interface position with annealing time.

The results are given in Fig. 12 as a function of the temperature and for the three orientations. The velocities are very close along the [100] and [110] and smaller along [111].

According to the classical theory of thermally activated growth,[14] the regrowth rate can be written as

$$v = v_0 \exp\left(-\frac{E_0}{k_B T}\right)\left\{1 - \exp\left[-\frac{\Delta S}{k_B}\left(\frac{T_m - T}{T}\right)\right]\right\}, \qquad (3)$$

where v_0 is a prefactor, E_0 is the activation energy of the SPE regime, T_m is the melting temperature, and ΔS is the entropy difference between the solid and liquid phases. In the SPE regime, the right hand side term of Eq. (3) is negligible, and the rate follows an Arrhenius form,

$$v_{\mathrm{SPE}} = v_0 \exp\left(-\frac{E_0}{k_B T}\right). \qquad (4)$$

The values of v_0 and E_0 have been calibrated for the [100] direction using both Olson's measurements[1] and our calculations up to a temperature of 2000 K to ensure a wider temperature range and, consecutively, a better precision on the activation energy in particular. The fit is shown in Fig. 2. The resulting activation energy is E_0=2.87 eV, in accordance with the experimental range from 2.4 eV by Csepregi *et al.*,[2] 2.75 eV by Olson and Roth,[1] to 2.9 eV by Drosd and Washburn.[3] The prefactor is $v_0^{[100]}=1.7\times10^7$ m/s. The fit is also reported in Fig. 13. Afterward, the activation energy E_0 is maintained constant for the three directions as no theoretical argument justifies a variation and as experimentalists get a constant value.[2,3] In these conditions, the two prefactors $v_0^{[110]}=1.7\times10^7$ m/s and $v_0^{[111]}=1.2\times10^7$ m/s are determined by fitting an Arrhenius law (Eq. (4)) on the temperature range of [1700–2000 K]. The melting temperatures, on the other hand, are calculated by molecular dynamics. The determination is made with a box formed of half liquid and half solid equilibrated at a fixed temperature. Below the melting temperature, the interface propagates toward the liquid. Above, the interface moves toward the solid. The melting temperature is at the transition between the two regimes. The values obtained in this way are 2510 K for the [100] and [110] boxes and 2490 K for the [111] box, with an error of ±20 K. A reduced melting temperature along [111] had already been measured by Ivlev and Gatskevich.[15] Using Eq. (3) enables us to fit the molecular dynamics calculation, as evidenced by Fig. 13. The values of $\Delta S/k_B$ deduced from this fit are 5.1, 5.3, and 3.6 for the [100], [110], and [111] directions, respectively.

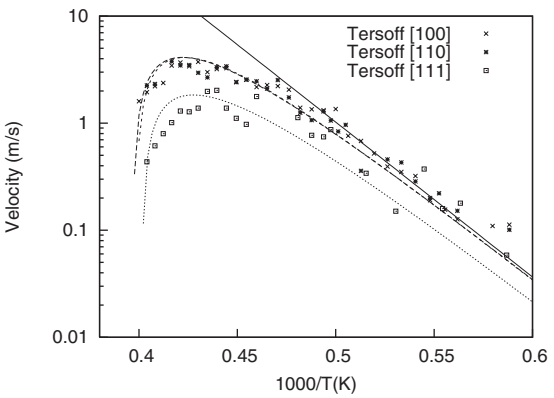

FIG. 13. Fit of the velocity along the three directions according to Eqs. (3) and (4).

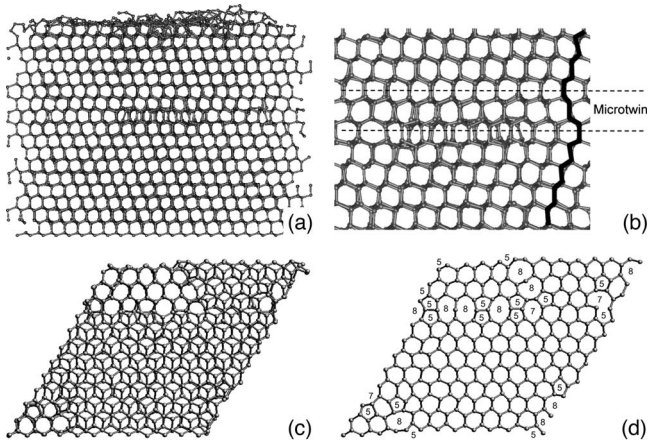

FIG. 14. Buried defect obtained after annealing at 1850 K of the [111] system. Section (left) and plane view (right).

V. DEFECTS

The annealing of [111] boxes systematically results (at only one exception over 42 cases) in the formation of one or more twins. An example is shown in Fig. 14(b), where two of these stacking faults are evidenced by the dark zigzag line at the right side. Indeed, the first neighbor distances are identical and the angles are undistorted in the twin configuration. Therefore, the difference in energy is expected to be negligible compared to the thermal energy, which could explain their frequent formation. The order within the bilayer being correct, as well as the distance with the underneath and above bilayers, we did not rule out the [111] configurations with twins for the calculations of the velocities presented in the previous section.

Apart from the twins, the SPE regrowth sometimes produce defects. The defects mainly occur at low temperatures. Their frequency of appearance is high for the [111] box (52%), smaller for the [110] (19%), and very low for the [100] box (8%). The defects are of two main kinds: (i) (111)

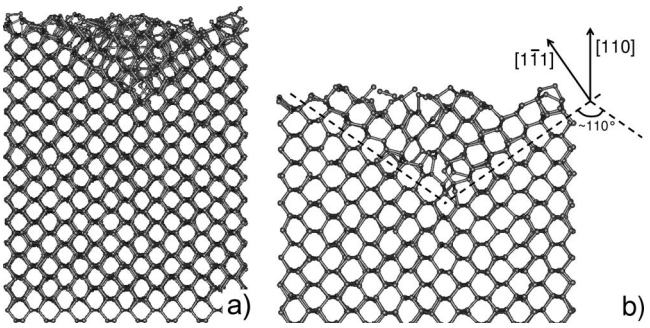

FIG. 15. Two views of the crystallization defect formed at 1750 K in the [110] oriented system.

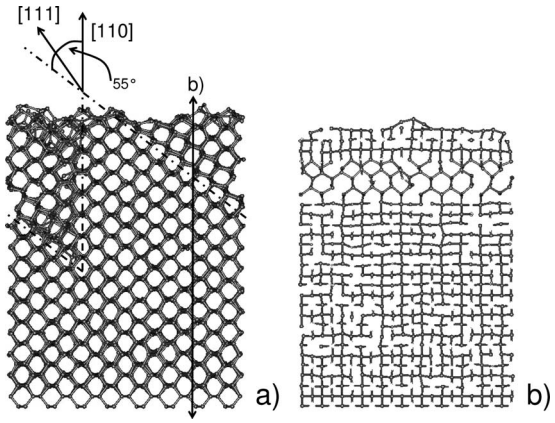

FIG. 16. Two views of the crystallization defect formed at 1800 K in the [110] oriented system. The location of the slice presented in view (b) is specified in view (a).

in-plane defects observed on [111] boxes and (ii) misoriented crystalline grains observed in the three cases.

The first category is illustrated in Fig. 14. The annealing temperature applied to this [111] box is 1850 K. In Fig. 14(a), the section of the entire structure after regrowth is given. A defect is visible at approximately midheight of the structure, with a length equal to the third of the box width. The defect involves two bilayers. Figure 14(b) is a zoom on the defect and the neighboring bilayers. Figure 14(c) is a plane view obtained by the superimposition of the two bilayers containing defects and a third perfect one. If the periodic boundary conditions are used to bring closer the various parts of the defect, a triangular shape is observed. Figure 14(d) is a plane view of one of the two bilayers containing the defect. This view evidences that the outline of the triangle is formed of five- and eightfold rings and sevenfold rings at the corners. Similar triangular defects were also obtained by Itoh[16] in his study of the Si (111) homoepitaxy. Five-, seven-, and eightfold rings are also observed in {113} defects induced by electron irradiation or ion implants.[17] In our calculations, other defects of the same kind were observed at other temperatures, having in common a rearrangement of atoms inside the bilayer.

The second kind of defects was observed in the three orientations. These defects are formed of misoriented crystalline regions. Indeed, misoriented regions after SPE were already suspected by Cerva and Küsters[18] to act as precursors of hairpin dislocations. Here, a first example obtained in our calculations is given in Fig. 15. The defect formed upon annealing the [110] box at 1750 K. View (a) is obtained with all the atoms while layers have been clipped at the foreground and the background to isolate the interface structure in view (b). Figure 9 shows the annealing conduct to the [111] faceting of the amorphous/crystalline interface. When the facets emerge at the surface, the triangular region in between does not cure even during ten times the duration required for the facets to reach the surface. It seems like the facets, perhaps containing defects and/or twins, and the presence of the surface, probably acting as a particular sink for stress, combine their effects to allow this recrystallization in a misoriented direction.

Another geometry of misoriented defects is shown in Fig. 16. The defect formed upon annealing of the [110] box at 1800 K. View (a) proves that the defect is delimited on one side by a vertical (100) plane and on the other side by a plane tilted of 55°. The location of the cross section presented in view (b) is also specified. View (b) evidences a twinned crystalline region that separates the bottom bulk crystal from the top. Smaller misoriented regions or aggregates, containing less than ten atoms, were also observed.

VI. DISCUSSION

Drosd and Washburn[3] proposed a phenomenological picture of the SPE regrowth based on successive completions of sixfold rings of atoms at a perfect crystalline interface. These sixfold rings are presented in Fig. 17 for the three interfaces ((100), (110), and (111)). Depending on the orientation of the

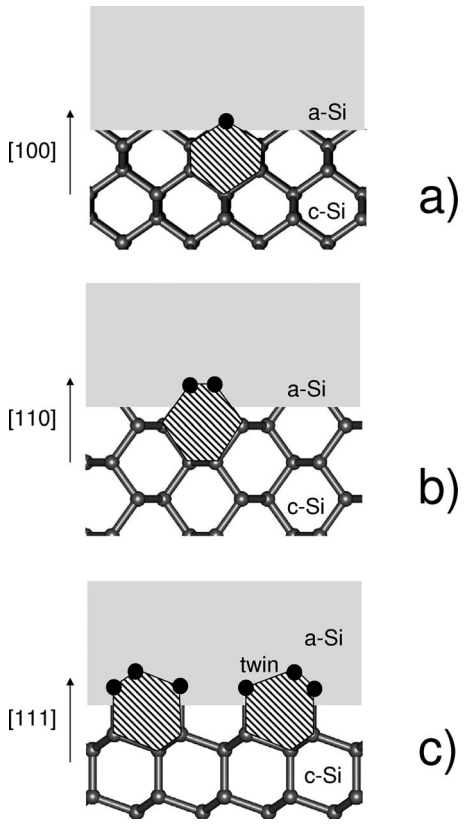

FIG. 17. Schematics of the sixfold ring model of Drosd and Washburn (Ref. 3) for the three orientations.

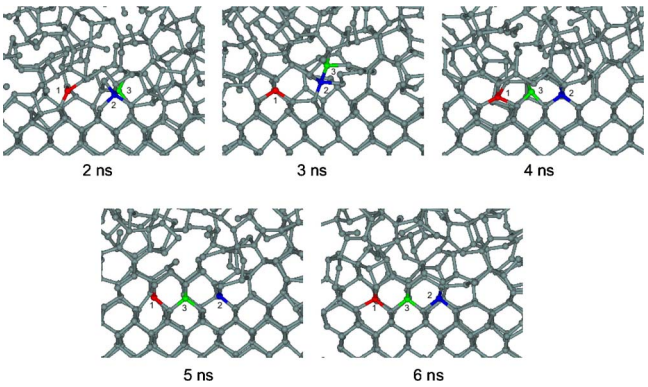

FIG. 18. (Color online) Motion of three atoms (#1 in red, #2 in blue and #3 in green) at the (100) a/c interface between 2 and 3 ns at 1725 K.

interface, the sixfold rings are lacking of one ([100] case), two ([110] case), or three ([111] case) atoms. The two consequences are that the velocity of the SPE regrowth should decrease and that the probability of forming defects increases from [100] to [110] to [111]. In particular, the triplet can be correct or twin at the (111) interface without expected unfilled bounds and, consecutively, with a high probability of formation. The decrease in the velocity from [100] and [110] to [111] and the increase in the occurrence of defects from [100] to [110] to [111] are obtained by molecular dynamics calculations, as shown in the previous sections. However, to test the assumptions made at the atomic level by Drosd and Washburn in more detail, we follow the motion of atoms at the amorphous/crystalline (a/c) interface during the incorporation. The calculations at 1725 K already presented in Figs. 8–10 are chosen for this purpose.

Figure 18 is a zoom of the motion of three atoms at the (100) interface. At 2 ns, the three atoms are in the disordered part. At 3 ns, the atom in red is incorporated in a sixfold ring, while the two others bond to adjacent rings at 4–5 ns. The picture by Drosd and Washburn is therefore observed in our molecular dynamics calculations. As a consequence of this process, the a/c interface remains planar during regrowth as shown at 6 ns.

The details of the (110) interface are presented in Fig. 19. At 1.5 ns, the interface is already faceted. Four pairs of atoms are successively incorporated into the crystal at 1.5–2 ns (pink-light blue), 2.2–2.4 ns (orange-violet), 2.8 ns (yellow-blue), and 2.8 and 3 ns (red-green). The eight atoms fulfill sixfold rings by pairs, as assumed by Drosd and Washburn, and the process obviously propagates the facet. Such a regrowth mechanism is accounted for the nanofaceting of the interface and the generation of defects at the corners of source/drain regions by Saenger *et al.*[19] in their model.

Finally, an example of the (111) interface evolution is reported in Fig. 20. Five atoms initially in the amorphous part make and break bonds in order to form a first triplet (atoms blue, yellow, and violet) at 7.6 ns and a second neighboring one (red, green, and yellow) at 7.8–8 ns. The front of crystallization therefore progresses by bilayers. At 8 ns, reconstructed sixfold rings begin to form on top of the two above rings, in coherence with the observation of partial regrowth bilayers in Fig. 10.

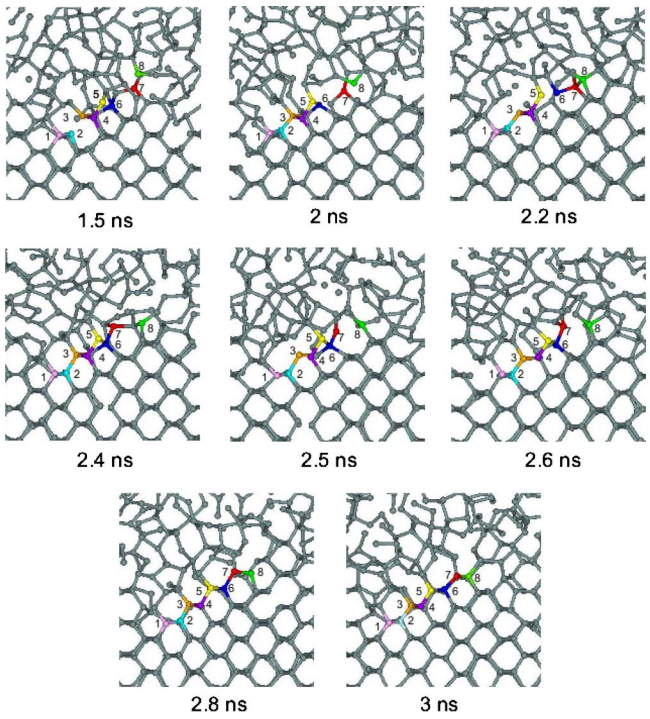

FIG. 19. (Color online) Motion of eight atoms (#1 in pink, #2 in light blue, #3 in orange, #4 in violet, #5 in yellow, #6 in blue, #7 in red and #8 in green) at the (110) faceted a/c interface between 1.5 and 3 ns at 1725 K.

VII. CONCLUSION

The molecular dynamics calculation of the SPE regrowth was reported in this work for [100], [110], and [111] directions. The regrowth proceeds by a motion of a planar a-Si/c-Si interface for [100], while the interface is nanofaceted for [110]. The regrowth of the [111] box is based on the reconstruction of the crystal within (111) bilayers. The velocities of SPE regrowth were furthermore extracted when the crystallized layer is defect free. The velocities are similar along [100] and [110] and two to five times lower along [111]. The occurrence of defects increases from [100] to [110] to [111]. Finally, the mechanisms proposed by Drosd and Washburn are evidenced at the atomic level. The atomistic picture of the initial stage of SPE provided by the

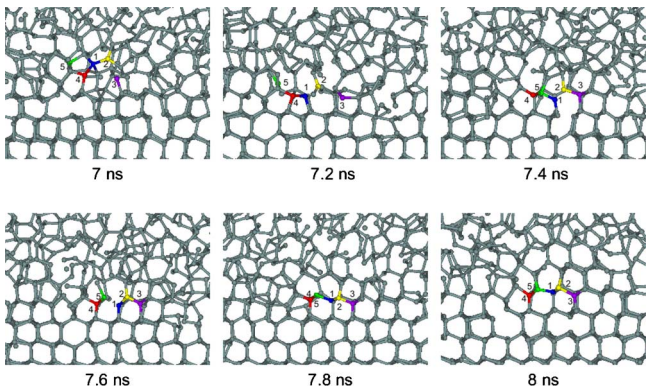

FIG. 20. (Color online) Motion of four atoms (#1 in blue, #2 in yellow, #3 in violet, #4 in red and #5 in green) at the (111) a/c interface between 7 and 8 ns at 1725 K.

present study could help to understand defect formation when silicon is amorphized in complex configurations[19] or in nanodevices.[20]

ACKNOWLEDGMENTS

The authors thank Fabrizio Cleri for the discussions on the molecular dynamics technique and the physics of silicon. They also thank Jean-Michel Droulez for the support on the computing aspects. This work was part of the integrated project PULLNano funded by the European community.

[1]G. L. Olson and J. A. Roth, Mater. Sci. Rep. **3**, 1 (1988).
[2]L. Csepregi, E. F. Kennedy, J. W. Mayer, and T. W. Sigmon, J. Appl. Phys. **49**, 3906 (1978).
[3]R. Drosd and J. Washburn, J. Appl. Phys. **53**, 397 (1982).
[4]B. C. Johnson, P. Gortmaker, and J. C. McCallum, Phys. Rev. B **77**, 214109 (2008).
[5]V. Cuny, Q. Brulin, E. Lampin, E. Lecat, C. Krzeminski, and F. Cleri, Europhys. Lett. **76**, 842 (2006).
[6]S. Munetoh, K. Moriguchi, A. Shintani, K. Nishihira, and T. Motooka, Phys. Rev. B **64**, 193314 (2001).
[7]C. Krzeminski, Q. Brulin, V. Cuny, E. Lecat, E. Lampin, and F. Cleri, J. Appl. Phys. **101**, 123506 (2007).
[8]F. Wooten, K. Winer, and D. Weaire, Phys. Rev. Lett. **54**, 1392 (1985).
[9]J. Tersoff, Phys. Rev. B **38**, 9902 (1988).
[10]E. J. Albenze and P. Clancy, Mol. Simul. **31**, 11 (2005).
[11]S. Nosé, Mol. Phys. **52**, 255 (1984).
[12]W. G. Hoover, Phys. Rev. A **31**, 1695 (1985).
[13]A. Mattoni and L. Colombo, Phys. Rev. B **69**, 045204 (2004).
[14]G.-Q. Lu, E. Nygren, and M. J. Aziz, J. Appl. Phys. **70**, 5323 (1991).
[15]G. D. Ivlev and E. I. Gatskevich, Appl. Surf. Sci. **143**, 265 (1999).
[16]M. Itoh, Phys. Rev. B **57**, 14623 (1998).
[17]S. Takeda, Jpn. J. Appl. Phys., Part 2 **30**, L639 (1991).
[18]H. Cerva and K.-H. Küsters, J. Appl. Phys. **66**, 4723 (1989).
[19]K. L. Saenger, J. P. de Souza, K. E. Fogel, J. A. Ott, C. Y. Sung, D. K. Sadana, and H. Yin, J. Appl. Phys. **101**, 024908 (2007).
[20]R. Duffy, M. J. H. Van Dal, B. J. Pawlak, M. Kaiser, R. G. R. Weemaes, B. Degroote, E. Kunnen, and E. Altamirano, Appl. Phys. Lett. **90**, 241912 (2007).